Experimental studies of Single-sided Ventilation for Semi-enclosed models with Horizontal Opening

Yuanyuan Lin[1*], *Mats* Sandberg[1], *Mathias* Cehlin[1], *Leif* Claesson[1], and *Hans* Wigö[1]

[1]Department of Building Engineering, Energy Systems and Sustainability Science, Faculty of Engineering and Sustainable Development, University of Gävle, 801 76, Gävle, Sweden

Abstract. As a preliminary investigation of the wind-driven purging process for densely built environments through the canopy layer, the ventilation efficiency of standalone semi-enclosed models incorporating a horizontal opening in the roof façade was investigated in the wind tunnel. For comparison, two models with different geometries were constructed, and each model was tested individually. Both models were equipped with replaceable roof covers, enabling the adjustment to the opening size. The ventilation efficiency was evaluated by continuous releasing and sampling of the tracer gas, from which the normalized purging velocity (*PFVn*) was derived. Additionally, the flow condition over the opening was monitored using the Laser Doppler Anemometer (LDA). It was found that separation flows from the frontal edge(s) of the model could introduce secondary circulations across large openings, resulting in dramatic increases in *PFVn*. Both the rectangular prism model and cylinder model possessed higher *PFVn* compared to prior studies on single-sided ventilation, while close values were observed with cylinder model mounted under the wind tunnel floor. Besides, the vertical distribution of integral length scales of streamwise velocity indicated the stratification feature of separation flows under low-turbulent incoming flow conditions. Measurement results provide validation data for further simulation studies including more detailed structures.

1 Introduction

Compact urban morphologies impose strong resistance to the ambient wind from the rural surroundings and deteriorate the city ventilation efficiency. Given an extreme scenario where there is no horizontal air movement within the street networks to remove the pollutant, the “opening” of streets at the roof height of buildings aside is a vital pathway for the pollutant removal, and a supply of fresh air. The vertical movements of air within urban regions are mainly driven by mechanical driven forces generated by wind, and density differences resulting from uneven solar heating or evaporation [1,2]. In this study, the mechanical driven by the external wind is primarily focused.

When there is a high velocity gradient between the external and internal air of a space, a shear layer forms near the boundary. Existing studies elaborate the generation and function of the shear layer at the roof level of street canyons for air exchange [3,4]. However, due to 2D simplification, it is challenging to reproduce disturbances from the surrounding structures, such as the separation flows from the buildings. Therefore, an idealized 3D semi-enclosed model is preferred with the aim to stress the impacts from disturbed flow by built structures, which is non-negligible in reality. As a precursor test, the single-sided ventilation for standalone semi-enclosed models with different horizontal openings in the roof façade is investigated in the present study.

Several factors were considered in the experiments, including orientations and geometries of the models, configurations of the openings, and incoming flow conditions. Two semi-enclosed models with different geometries were designed and tested individually for comparative studies, both features replaceable roof covers with various openings. Tracer gas measurements were conducted with a long-time releasing and sampling method to assess the ventilation efficiencies under different conditions. Additionally, velocities over the opening center were monitored by a 2D Laser Doppler Anemometer (LDA) system in high frequencies. The ventilation through a vertical opening parallel to the incoming flow (e.g. windows in lateral facades) has been extensively investigated in many studies focusing on the building ventilation, with many of them also conducted wind tunnel experiments with similar isolated models [5–7]. While few studies have attempted to explore the single-sided ventilation for semi-enclosed spaces with horizontal opening at roof level (e.g. [6,8]). Therefore, our experiments can also serve as a preliminary study for comparison.

2 Model designs and Methods

* Corresponding author: yuanyuan.lin@hig.se

2.1 Model designs

Experiments were conducted in a closed return-flow wind tunnel at the University of Gavle, Sweden. The working section of the wind tunnel measures 3 m wide, 1.5 m high, and 11 m long. The entire tunnel is elevated to accommodate facilities mounted under its floor. The floor of the working section features a turntable with a diameter of 3 m, which can be precisely controlled by a computer.

The geometry information of the two semi-enclosed models, including the replaceable roof covers with various openings and relevant settings for the wind tunnel experiments, are depicted in Fig. 1-2. The first model is shaped like a rectangular prism as shown in Fig. 1 (referred to as 'box' subsequently for brevity). The box was orientated from 0° to 90° in 15° intervals relative to the incoming flow, to create various separation flow conditions (Fig. 1d). The second model, resembling a cylinder, is of equal height to the box (Fig. 2). The cylinder model was test in two positions, either standing on or mounted beneath the floor of the working section, with the purpose of comparing the purging efficiency considering the presence or absence of the blocking effect and the consequent separation flow (Fig. 2d). Additionally, both models possess a replaceable roof cover with a single opening in diverse sizes and shapes (Fig. 1c and Fig. 2b), which was designed to investigate potential effects of the porosity.

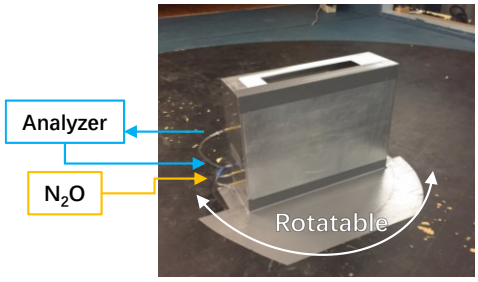

(a)

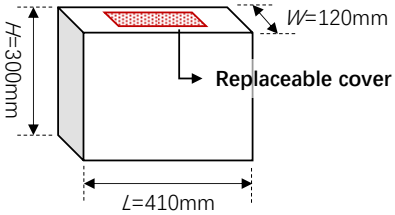

(b)

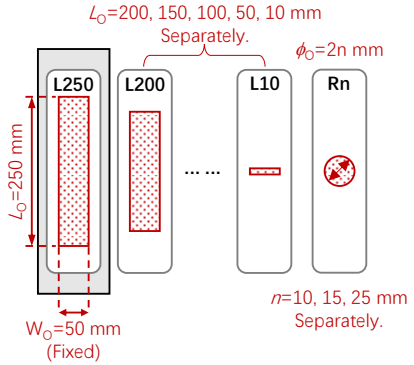

(c)

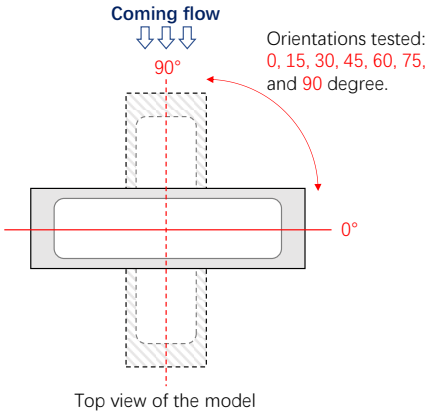

(d)

Fig. 1. Sketches of the rectangular-prism model, showcasing (a) the model with the tracer gas releasing and sampling system, (b) geometry information, (c) specifics of openings in replaceable roof covers, and (d) the relative orientations of the model to the incoming flow.

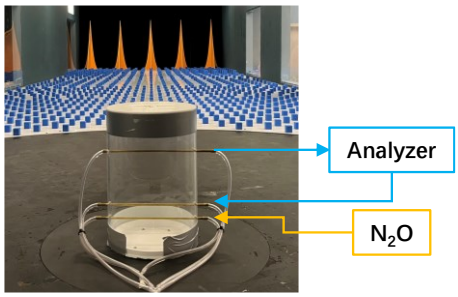

(a)

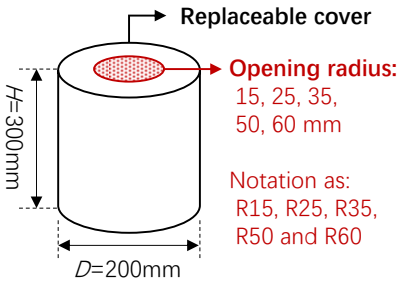

(b)

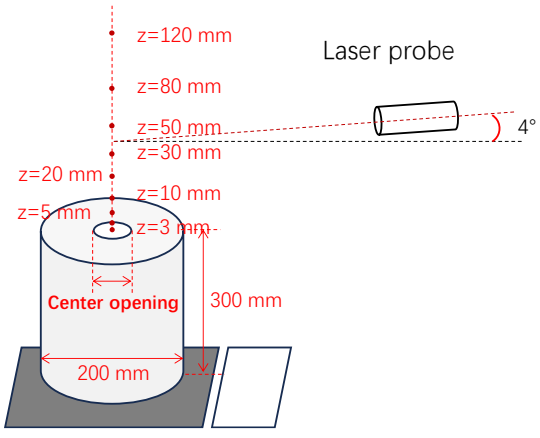

(c)

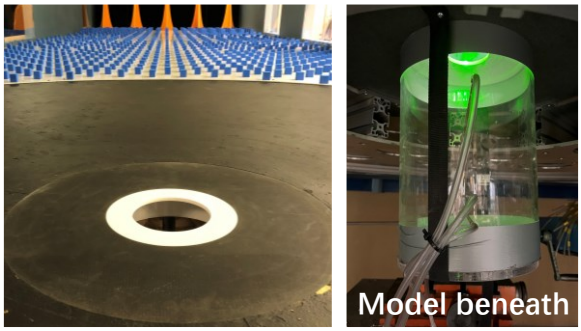

(d)

Fig. 2. Measurement settings with the cylinder model. (a) The model with the tracer gas releasing and sampling system. (b) Geometry information of the cylinder model. (c) Measurement positions for the 2D Laser Doppler Anemometer (LDA) system with the model standing on the floor. (d) Photos depicting the cylinder model mounted beneath the floor level of the working section, with model's roof aligned with the floor.

2.2 Tracer gas measurements

A long-time continuous releasing method with N_2O gas was adopted. As shown in Fig. 1a and 2a, the tracer gas was slowly released from a porous tube going through the lower quarter section of the model, while the analyzer sampled and returned the gas in the upper section of the model. The holes in the tubes are small enough to eliminate the initial momentum from the release. Before commencing the data recording, the flow rate of the tracer gas would be adjusted to a favorable value that maintained a stable concentration around 100 ppm within the model. Then the concentration inside the model would be recorded every 3 seconds and continued for 10 minutes for each case. Background concentration in the wind tunnel was subtracted simultaneously. Based on the measured concentration and the stable releasing rate, an equivalent purging efficiency can be derived, which accounts for the purging effects by bidirectional movements of air across the horizontal opening.

2.3 Velocity measurements

Due to page limitation, only the velocity measurements conducted with the cylinder model standing on the floor are discussed here.

The velocity above the center of the opening were monitored by a 2D Laser Doppler Anemometer (LDA) system manufactured by Dantec Inc., for which the inherent uncertainty is 0.07% [9]. Data was recorded and processed by the accompanying software. The Burst mode was employed to acquire velocity data at sufficient high frequencies, wherein the velocity is recorded when a burst signal from the reflection of the passing particle is detected. Therefore, the time interval between each sample is ununiform, while we maintained the average sampling frequency beyond 1000 Hz. Moreover, to measure as close to the model top as possible, the laser probe was positioned at a slight downward angle of 4°, as depicted in Fig. 2c. Besides, with a long focal length of 400 mm for the frontal focusing lens, the laser probe maintained a sufficient distance from the model, minimizing interruptions to the flow around it.

Two orthogonal components of the velocity were monitored: the streamwise component (u_1) and a resultant component (u_2). Due to the minor incline angle of the laser probe at 4°, the component u_2 predominately represents the vertical velocity (w), but inevitably includes a part of projection of the spanwise velocity (v).

2.4 Incoming flow conditions

With dismountable spires and roughness elements in the upstream section of the wind tunnel, two different incoming flow conditions can be produced: *turbulent flow* and low turbulence *smooth flow*. The profiles of normalized mean velocity ($U/U_{z=1m}$) and turbulence intensity (i.e. ratio of root mean square of the velocity to the mean, U_{RMS}/U) for two conditions are illustrated in Fig. 3. In addition, three turbine speeds, 300, 500 and 700 rpm (i.e. revolutions per minute) for the wind tunnel fans, were adopted in this study, corresponding to velocities at model height (U_H) of 8.93, 15.27, and 21.68 m/s for smooth flow condition (Fig. 3a), and 6.56, 11.1, and 15.83 m/s under turbulent flow conditions (Fig. 3b).

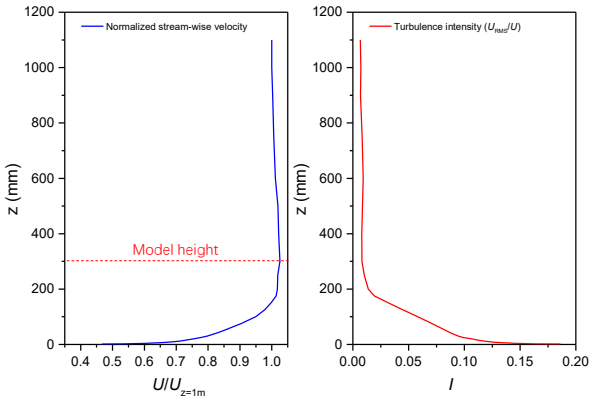

(a)

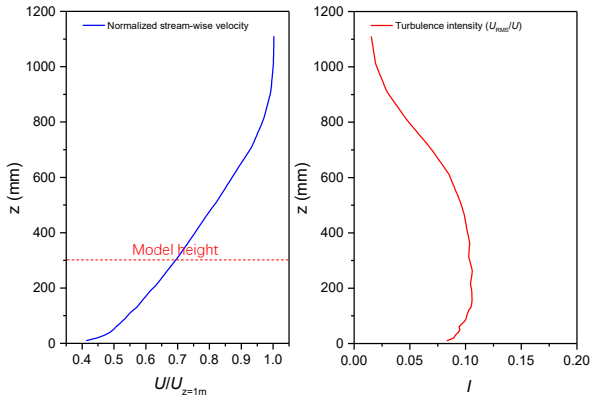

(b)

Fig. 3. Normalized wind velocity and turbulence intensity profiles depicted for (a) smooth flow condition, and (b) turbulent flow condition.

2.5 Evaluation Quantity for Purging Efficiency

The purging flow rate (PFR) indicates the equivalent net flow rate that contributes to the removal of pollutant,

which is defined as Eq. 1 [10]. To compare the purging efficiency between cases with diverse openings and incoming flow conditions, the purging flow rate (*PFR*) was normalized by the opening area (A_O) and the incoming flow velocity at model height (U_H), as shown in Eq. 2. This dimensionless quantity is denoted as normalized purging velocity (*PFVn*) in the subsequent.

$$PFR = q_p/(C_p \times \rho_{air}) \quad (1)$$

$$PFVn = PFR/(A_O \times U_H) \quad (2)$$

In above equations, the variables are defined as follows: q_p is the mass release rate [kg/s], C_p is the spatial mean concentration in fraction [kg/kg], ρ_{air} is the density of the air (1.2 kg/m^3, at 20°C, 1 atm).

Our results are compared with those from two typical studies on the single-sided ventilation: Kato et al. (2006) and Chu et al. (2011) [6,7]. Fig. 4 illustrates the case settings of the two selected cases from literature for comparison. In Chu et al. (2011), a dimensionless ventilation rate Q^* was introduced, which is derived based on the tracer gas decay method [7]. While in Kato et al. (2006), with long-time releasing method, a similar dimensionless parameter is defined, named k in their research [6]. The quantity *PFVn* is mathematically identical with these two parameters. However, the experimental method used to obtain the purging flow rate for calculating Q*, and the reference velocity used for normalization of k are different from ours. For the sake of precision, we chose not to adopt the same name for the dimensionless quantity as what used in these two studies.

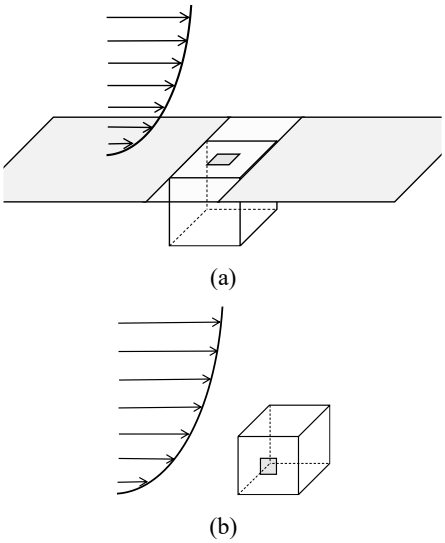

(a)

(b)

Fig. 4. Brief sketches of the experiments selected for comparison from (a) Kato et al. (2006) [6], and (b) Chu et al. (2011) [7].

3 Results

3.1 Purging efficiency of the rectangular prism model under different conditions

The *PFVn* results obtained with different incoming flow velocities with the box model are presented in average values for brevity. Additionally, the dimensionless ventilation rates from the studies on the shear-induced single-sided ventilation by Kato et al. (2006) [6] and Chu et al. (2011) [7] are also indicated by dashed lines in diagrams for comparison.

Fig. 5 illustrates the variation of *PFVn* for each opening with orientation, separately with the smooth turbulent incoming flow. Comparing Fig. 5a and 5b, it can be learnt that the turbulent incoming flow generally induces more efficient purging through the horizontal opening in the roof façade when the box model was orientated from 0° to 45°. In contrast, larger openings (e.g. opening L150 and L250) experienced a sharp increase in the *PFVn* value when the model was orientated at 75° or 90° with smooth incoming flow. The ascending of *PFVn* values with large opening results from a secondary circulation penetrating deeply into the model, benefiting from a favorable distance between the opening and the frontal edge of the model, which was reported in our previous study utilizing particle image visualization (PIV) method [11]. In addition, the evident differences between the *PFVn* values with different incoming flow conditions at 45° suggest varying flow separations over the model roof. When the model was orientated at 75°, the incoming flow direction was nearly parallel to the diagonal axis of the box. Except for the largest opening L250 under smooth flow, most cases had minimal impact on the surrounding flow at this orientation, resulting in low *PFVn* values.

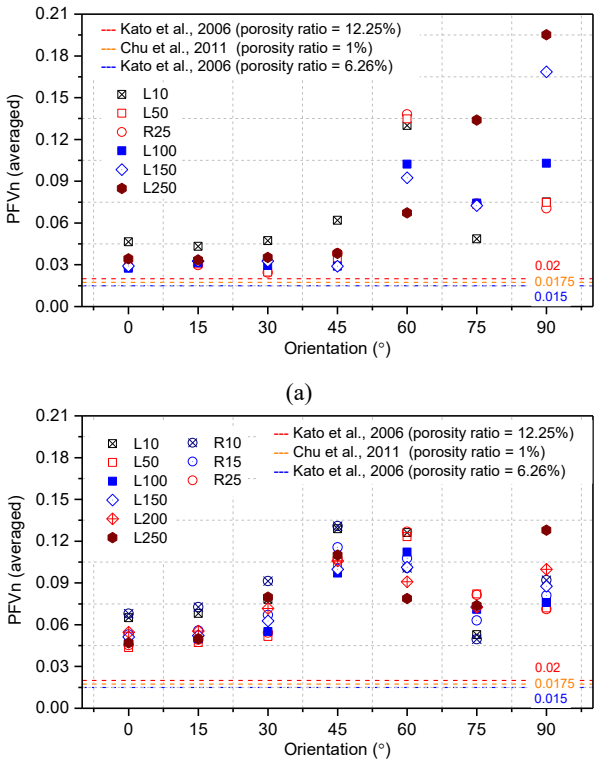

Fig. 5. The averaged *PFVn* for each opening with the box model tested with three different incoming flow velocities, under (a) smooth incoming flow condition, and (b) turbulent incoming flow condition.

The relation between the wall porosity and *PFVn* at different orientations are shown in Fig. 6. Porosity is

defined as the ratio between the area of the opening and area of the façade it is located:

$$Porosity\% = A_{opening}/A_{facade} \times 100\% \quad (3)$$

The trends in *PFVn* with increasing porosity exhibit uniformity with orientations from 0° to 45° with smooth flow, and at 0° and 15° with turbulent flow, aligning with the results depicted in Fig. 5. When the box model is orientated at 60° under both incoming flow conditions, the value of *PFVn* shows a monotonic decrease when the porosity exceeds 4%. And the dramatic increases in *PFVn* with increasing porosity are noticeable under smooth flow conditions at orientation of 75° and 90°. In addition, the low porosity ratios (associated with opening L10 and R10) shows higher *PFVn* compared to medium porosity ratios. This implies a different pattern of interaction between the small horizontal openings and the overlying flow, which needs further investigation. Finally, and most importantly, all the *PFVn* values presented above are higher than those in the literature, across the wide range of porosity ratios tested.

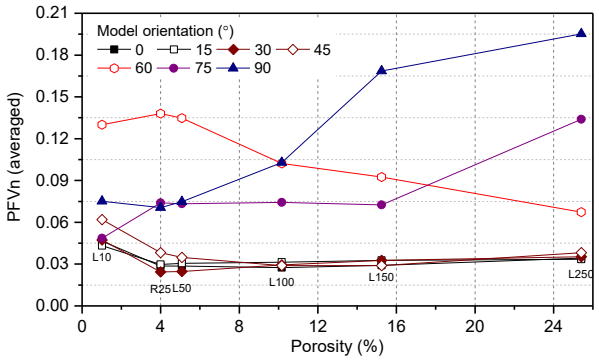

(a)

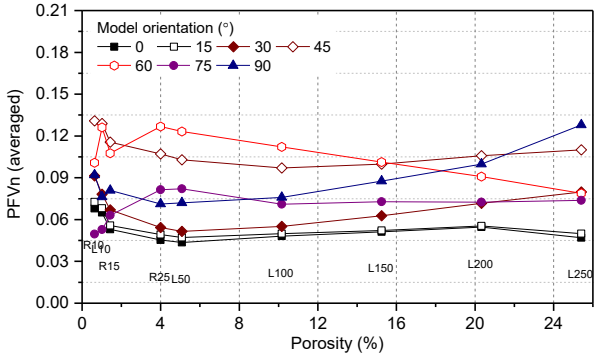

(b)

Fig. 6. The averaged *PFVn* for each opening with the box model at different wall porosity ratios under (a) smooth incoming flow condition, and (b) turbulent incoming flow condition.

3.2 Purging efficiency of the cylinder model under different conditions

The *PFVn* values obtained with the cylinder models standing on the floor are illustrated in Fig. 7. The turbulent incoming flow brought a more pronounced enhancement of *PFVn* compared to that with the box model. *PFVn* values in most cases demonstrate sufficient independence from the incoming flow velocity, expect for the largest opening R60 under smooth flow condition. Besides, the trend of *PFVn* with increasing porosity under turbulent flow resembles a mild increasing concave function, as shown in Fig. 7a, whereas under smooth flow condition, it resembles a convex function, as depicted in Fig. 7b. All *PFVn* values derived are higher than that in the literature.

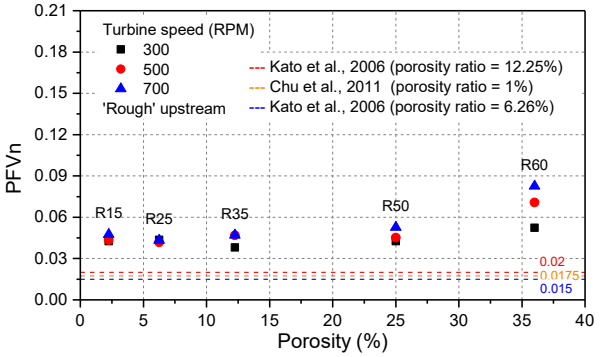

(a)

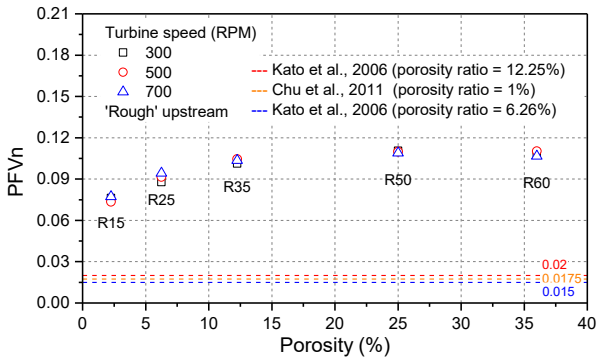

(b)

Fig. 7. The *PFVn* for each opening with the cylinder model tested under distinct incoming flow velocities, under (a) smooth flow conditions, and (b) turbulent flow conditions.

The *PFVn* with cylinder model mounted under the floor are presented in Fig. 8. Such model setting closely resembles the experiments conducted by Kato et al. (2006). And our results demonstrate high consistence compared to their nondimensional purging efficiencies when the porosity ratio exceeds 10%, which implies the particular impact of the blocking effects and separation flows to the purging process through the horizontal opening in the roof façade when model is standing on the floor.

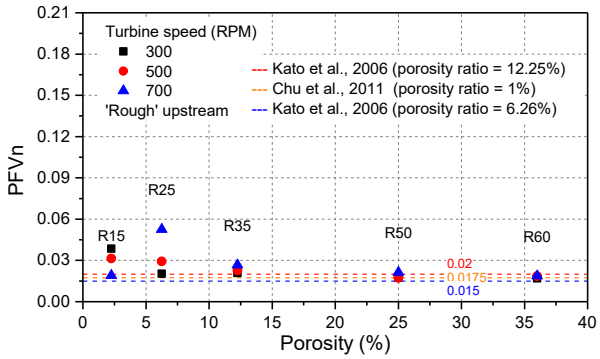

(a)

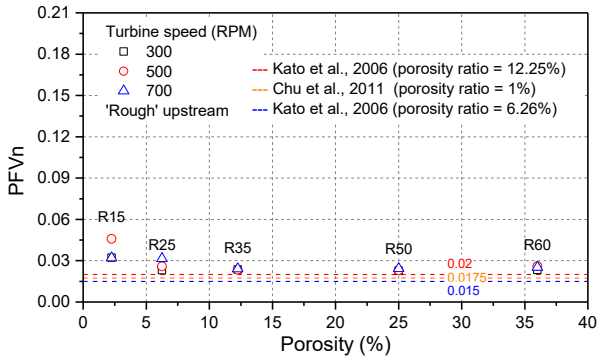

(b)

Fig. 8. The *PFVn* for each opening with the cylinder model mounted beneath the wind tunnel floor, under (a) smooth flow conditions, and (b) turbulent flow conditions.

3.3 Turbulence characteristics of the flow overlying the cylinder model standing on the floor

The autocorrelation was calculated separately for the two velocity components, the streamwise component (u_1) and the resultant component (u_2), with the maximum time lag as 200 ms. Resampling of 16384 data from the original time series was conducted for the calculation. Normalization was applied.

As shown in Fig. 9, with smooth incoming flow, the autocorrelation coefficients feature a negative peak value at a very short time lag around 5 ms, which does not exist when the model was sealed (Fig. 9a) and is enhanced by the increasing of opening size. It is noteworthy that such distinct negative peaks are mainly captured at 50 mm, regardless of the size of the opening. The resultant component u_2 also has similar features. For brevity, only autocorrelation results of the streamwise component u_1 collected with medium turbine velocity (500 rpm) are presented in Fig.9.

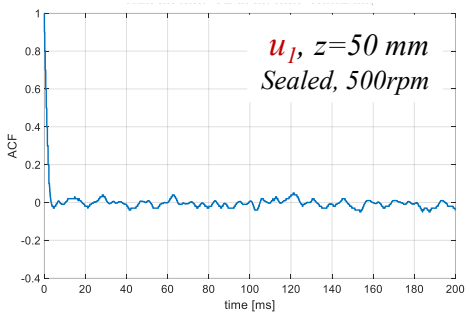

(a)

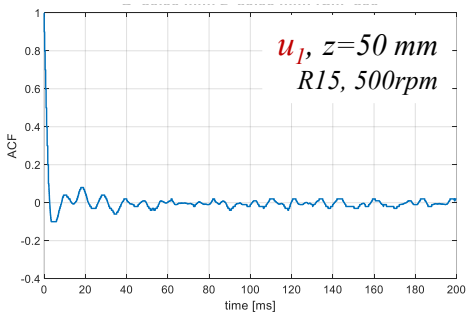

(b)

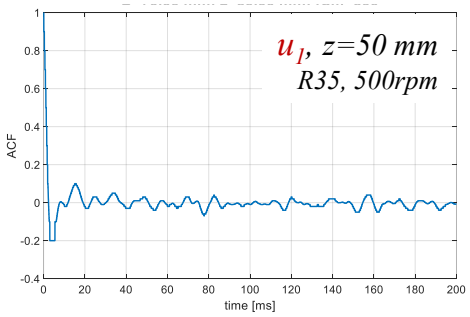

(c)

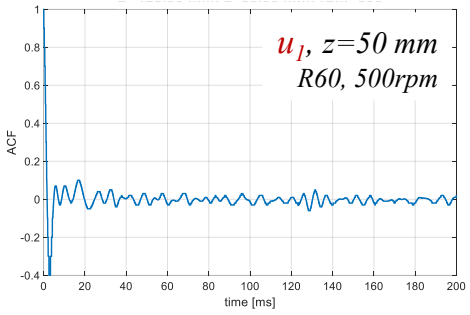

(d)

Fig. 9. The autocorrelation function (ACF) plots for selected cases, calculated by streamwise component u_1 at z=50 mm under smooth incoming flow condition, with a turbine speed of the fans as 500 rpm.

In contrast, for all openings under turbulent flow condition, no significant peak in the autocorrelation coefficients is observed for u_1, when compared to the results derived with the sealed condition. However, the coefficients of the resultant component u_2 present strong fluctuations, particularly for measurements with small openings at positions close to the model roof. And the intensity of the fluctuations is influenced by the incoming flow velocity, as illustrated in Fig. 10 with typical cases. Additionally, autocorrelation coefficients of the resultant component u_2 exhibit negative peaks at short time lag with larger openings (opening R50 and R60), which can be found across a wide range of distance from the model roof (figures are omitted due to page limitation).

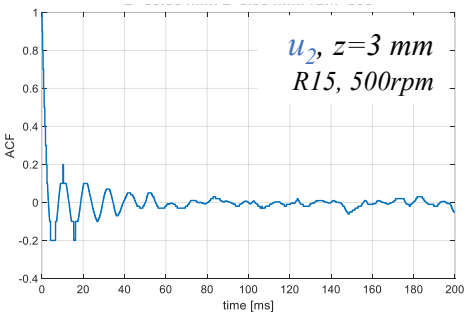

(a)

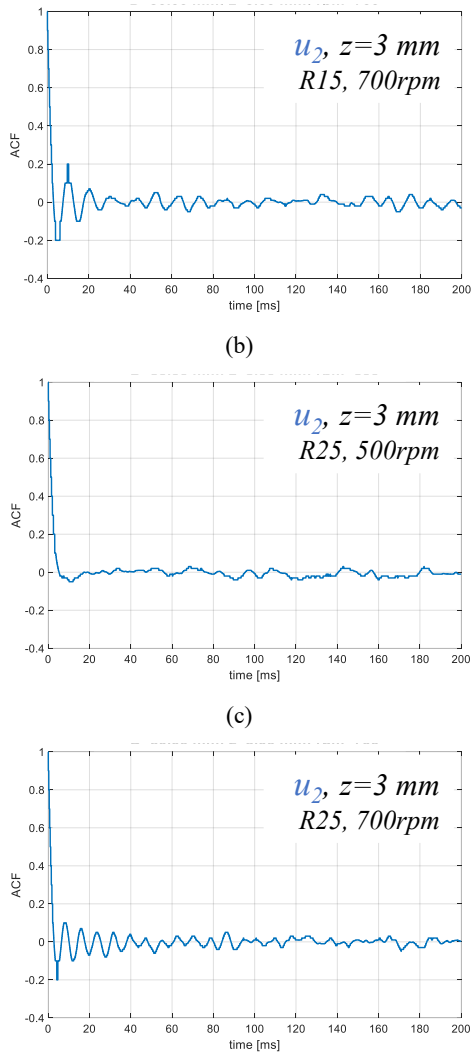

Fig. 10. The *ACF* plots of u_2 at z=3 mm for small openings R15 and R25 under turbulent wind conditions with different velocity magnitudes.

The integral length scale of velocity fluctuation is calculated based on the Taylor's hypothesis. To satisfy the frozen turbulence assumption, a high mean velocity is necessary. Therefore, the integral length scale is only calculated for the streamwise component u_1. The calculation is conducted with the integration from 0 to 100 ms of the autocorrelation function:

$$\lambda = \overline{u_1} \int ACF \, dt \tag{4}$$

The distribution of integral length scale along the height demonstrates similar trends across the three different incoming flow velocities. Therefore, only the results with medium turbine velocity 500 rpm are presented below in Fig. 11. The integral length scales normalized by the diameter of openings are also calculated.

In Fig. 11a, under the smooth incoming flow condition, a noticeable increasing in the length scale between heights at 50 mm and 80 mm is found, indicating stratification of turbulence conditions within the separation flow. Such a surge in the value of the integral length scale does not exist under turbulent incoming flow condition, which indicates the inherent turbulence within the incoming flow and its velocity gradient result in a different separation flow pattern overlying the model. Additionally, there is no strong dependence between the integral length scale of the velocity fluctuation and the geometry of openings, as evidenced by the normalized length scales depicted in Fig. 11c and 11d.

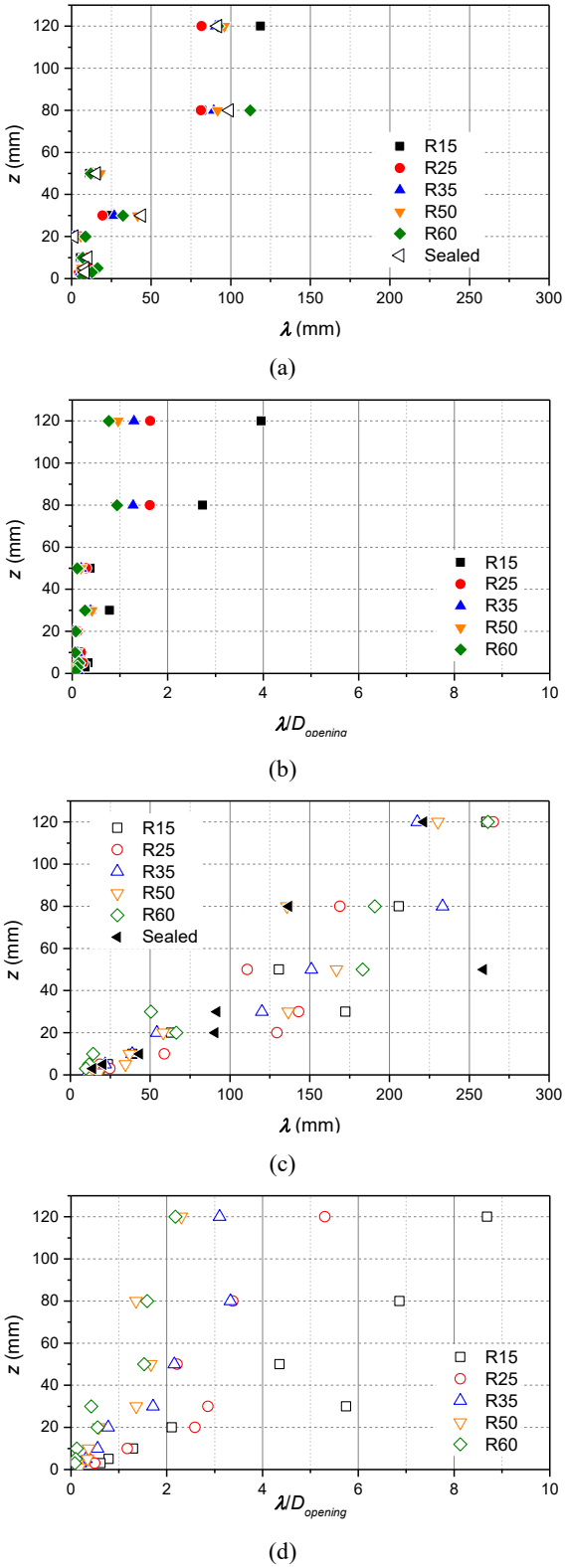

Fig. 11. Distributions of the integral length scales of the streamwise component u_1 along the height under (a) smooth incoming flow, and (b) turbulent incoming flow condition. The normalized integral length scale under (c) smooth

incoming flow, and (d) turbulent incoming flow condition. Calculated by data gathered with turbine speed of 500 rpm.

4 Conclusive Discussion

The single-sided ventilation for standalone semi-enclosed models with a horizontal opening in its roof façade was systematically studied from various aspects by wind tunnel experiments in this study.

The primary factor investigated is the varied separation flows induced by the obstruction of the model to the incoming flow. To address this aim, two models with distinct geometries were designed. The rectangular prism (box) model underwent measurements with various orientations, while the cylinder model was tested in two configurations: mounted on the floor or beneath it. Segmented characteristics of the trend between *PFVn* and orientations of the box model indicate the transformation of separation flow patterns, while the surge of *PFVn* with larger openings, when the model orientated at 75° or 90°, reveals the emergence of secondary circulation involving both the external and internal flow. For the cylinder model, significantly higher *PFVn* were obtained with the model placed on the floor, suggesting a general enhancement in purging efficiency by the separation flow over the horizontal opening.

The second consideration is the wall porosity, for which openings in different sizes were employed utilizing replaceable roof covers for both models. Besides the purging process driven by the secondary circulation across large openings, openings with very low porosity ratios exhibit relatively higher *PFVn* without direct flow impact. In specific, this was observed when the box model was orientated between 0° to 60°, or with the cylinder model placed beneath the floor.

The influence of incoming flow conditions was also explored. The turbulent flow typically leads to higher *PFVn* in most cases, with relatively minor discrepancies between different openings. Meanwhile, the surge in the integral length scales between z=50 and 80 mm implies stratification of the separation flow over the cylinder model under smooth flow condition.

It's noteworthy that, with model placed on the floor, our study gained much higher dimensionless purging efficiencies (*PFVn* here) compared to that reported in existing studies on the single-sided ventilation with opening in the lateral façade (e.g., Chu et al. (2011) [7]). However, close agreement was observed with the cylinder model mounted under the floor, a scenario similar to the experiment conducted by Kato et al. (2006) [6], where the incoming flow was undisturbed by the model. Moreover, While the two studies mentioned above reported very close dimensionless purging efficiencies despite the distinct model configurations as shown in Fig. 4. Such consistency in values between the referred studies suggests the necessity for further investigations.

This study was designed based on the assumption of a densely built urban region which was primarily ventilated by the flow over the buildings. Therefore, compared to most of the existing single-sided ventilation studies, diversities of the overlying flow conditions were stressed in our cases, which represents the complexity of urban flow. As a precursor study, it highlights distinct characteristics of the separation flow over the roof and its interactions with the horizontal opening. In addition, measurement results can be used as validation data for further simulation studies including more detailed urban structures. The results can also provide valuable insights for improving urban design, particularly with the context of compact cities.

Acknowledgement. This work has been financially supported by the Swedish government research council Formas (Grant nr. 2018–00238).

References

1. G. Chen, J. Hang, L. Chen, Y. Lin, Building and Environment, **244**, 110744 (2023)
2. A. Kubilay, D. Derome, J. Carmeliet, Sustainable Cities and Society, **49**, 101574 (2019)
3. F. Caton, R. E. Britter, S. Dalziel, Atmospheric Environment, **37**, 693–702 (2003)
4. J. Allegrini, Building and Environment, **143**, 71–88 (2018)
5. H.-Y. Zhong, Y. Sun, J. Shang, F.-P. Qian, F.-Y. Zhao, H. Kikumoto, C. Jimenez-Bescos, X. Liu, Building and Environment, **212**, 108797 (2022)
6. S. Kato, R. Kono, T. Hasama, R. Ooka, T. Takahashi, International Journal of Ventilation, **5**, 171–178 (2006)
7. C. R. Chu, R.-H. Chen, J.-W. Chen, Energy and Buildings, **43**, 2631–2637 (2011)
8. T. Van Hooff, B. Blocken, Computers & Fluids, **39**, 1146–1155 (2010)
9. Dantec Dynamics A/S, BSA flow software users guide, v6.71, (Dantec Inc., Denmark, 2019)
10. D. Etheridge, M. Sandberg, Building Ventilation: Theory and Measurement, (Wiley, 1996)
11. Y. Lin, M. Sandberg, M. Cehlin, L. Claesson, H. Wigö, *Evaluation of the Equivalent Purging Flow Rate for Single-Side Ventilated Model with Tracer Gas Measurements*, in Proceedings of the 5th International Conference on Building Energy and Environment, Springer Nature Singapore, COBEE, 25-29 July 2022, Montreal, Canada, (2022)